Flux−Force Formalism for Charge Transport Dynamics in Supramolecular Structures. 2. Diffusivity and Electroneutrality Coupling Effects

R. Aldrin Denny and M. V. Sangaranarayanan*

Department of Chemistry, Indian Institute of Technology, Madras-600 036, India

Received: September 24, 1997

The conductance and transport number expressions are derived for the ion-involved electron-hopping (IIEH) mechanism taking into account the ion pairing between fixed redox ions and the mobile electroinactive counterions. Under the steady-state condition, the effects of ion pairing, the ratio of diffusivity associated with electron hopping and the mobile electroinactive counterion, and the applied potential are studied both in the presence and in the absence of supporting electrolyte. The main effect of ion pairing is to decrease the charge transport rate, and that of the diffusivity rake is to change the mechanism of the conductance process from ohmic (electronic) to redox (or nonohmic). This change in the conductance behavior from ohmic to nonohmic is shown to be due to the change in the rate-limiting process from electron transport to counterion movement. A direct correlation between the proposed theory and experimental results obtained earlier using poly(benzimidazobenzophenanthroline) and $[Os(vbpy)^3]^{2+}/[Zn(vbpy)_3]^{2+}$ copolymer coated electrodes is demonstrated.

Introduction

Modified electrodes contain electroactive polymers which include π-conjugated type electronically conducting materials[1,2] having spatially delocalized electronic states distributed over a broad energy range (e.g., polyacetylenes, polypyrrole, and polythiophene and certain organometallic assemblies), redox polymers having electronically localized sites coupled covalently to the polymeric matrix[3−5] (e.g., polymeric metal bipyridines, viologens, quinones, and ferrocene), and ion-exchange polymers with mobile oxidation−reduction couples held electrostatically within the polymer (e.g., $Fe(CN)_6^{3-/4-}$ in protonated poly(4-vinylpyridine) and $Co(bpy)_3^{3+/2+}$ in Nafion). Electrodes can be coated with these electrochemically reactive polymers in several microstructural formats[6] (sandwich, array, bilayer, micro- and ion-gate electrodes). These microstructures are used to study transport of electrons and ions as a function of the polymer oxidation state, potential, solvent environment, etc., and are essential for understanding the conductivity properties of these materials.

Electron conduction observed in polymer film coated electrode surfaces can be classified into two categories: ohmic and redox.[7] Ohmic conductance is characterized by the linear dc current−voltage curves which are characteristic of electronically conducting polymers.[8−11] These polymers have double bonds that are highly conjugated and hence postulated to have bandlike electronic structures where conduction takes place. Conductivities observed for these electronic conductors range from 10^3 to 10^{-3} S/cm. Another form of charge transport conduction also exists and is termed redox conductivity.[12,13] Here, the mechanism of conduction is via electron self-exchange by thermally and electrically activated hopping between the oxidized and reduced species under the impetus of electrochemical potential gradients. The thermal activation barrier for redox conductors are nearly 10-fold larger than the electronic conductors and hence have much lower conductivity. The conductance−potential curves for redox conductors appear as an "inverted parabola", and hence they are nonohmic.

Several earlier studies[14−16] have emphasized counterion movement to contribute to the overall conductance of the polymer. The influence of various ions to the total conductivity in partially oxidized conducting polymers is in general not identical. These differences in conductivities are attributed either to the fundamental effect of the nature of the counterions on conductivity,[16−18] to the method of partial oxidation of the polymer,[19] or to conditions under which the conductivity studies are carried out.[7−13,20,21] Many independent theoretical calculations on the electronic structure of conducting polymers also suggest that the geometry of the counterions has a significant effect on the conductivity.

It is important to emphasize at this stage two different directions along which transport processes in polymer-modified electrodes are customarily investigated, viz., (i) assuming the flux of counterions to be zero while evaluating current and (ii) explicitly incorporating the contribution of counterion flux in the total conductance vis-à-vis impedance. The former approach has been advocated in particular by Savéant[22−26] and Murray et al.,[7,12,13] while the latter strategy is followed by Buck,[20,21,27−31] Mathias and Hass,[32,33] and Vos and co-workers.[34−36] Furthermore, the experimental data provided in the analysis of Forster et al.[34] employing chronoamperometry, chronocoulometry, and cyclic voltammetry clearly indicate the significant influence of counterions in dictating charge transport. We have resorted to the methodology of including counterion motion while expressing the rate of charge transport.

To unravel the details of the transport mechanism in polymer-modified electrodes, the theoretical concepts up to the present have been essentially restricted to specific models. In an earlier analysis, Saveant[24] studied the variation of conductance with the ion-pairing association constant and redox composition of the polymer for potential step (chronoamperometry) experiments, and Mathias and Hass[32] analyzed the effect of the diffusivity ratio of the electroactive and electroinactive ions and

S1089-5647(97)03318-X CCC: $15.00
Published on Web 03/03/1998

SCHEME 1

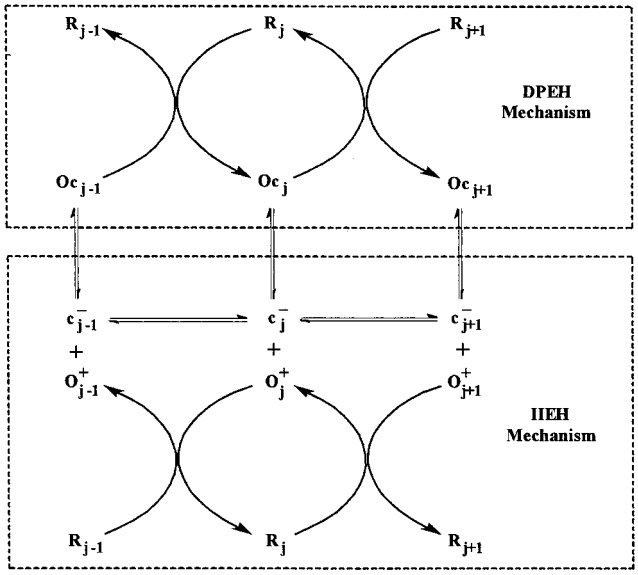

redox composition using impedance spectroscopy. However, conductance is a function of the extent of ion pairing, redox composition of the polymer, and the diffusion coefficients of electroactive ions and inactive counterions.[31] The variation of conductance with these three parameters has not yet been studied simultaneously. Here we report a new approach exploiting the concepts of irreversible thermodynamics which answers globally (almost all) the parametric dependences predicted earlier using specific models and provides a rational explanation for the observed patterns. In addition, new parameters hitherto unknown in this context can easily be devised, and their importance in the experimental studies to understand the complex transport mechanism delineated.

Ion Pairing and Conductance

The charge propagation in supramolecular structures is customarily assumed to proceed via electron hopping between oxidized and reduced species through bimolecular self-exchange reaction.[37] Owing to the ionogenic nature of the polymeric backbone and in view of the large ionic concentrations, extensive ion pairing and possibly higher ion aggregation are expected to occur in the redox polymeric system.[38,39] Thus, one can assume two different pathways by which electron transport can occur, the first one being the direct participation of both oxidized and reduced species (as ion pairs) in the electron-hopping process (upper half of Scheme 1). The second possibility is the non-ion-paired oxidized species (as ions) transferring electrons by self-exchange reaction with the reduced species. This mechanism is represented in the lower half of Scheme 1. We denote the former as the direct participation electron-hopping (DPEH) mechanism and the latter as the ion-involved electron-hopping (IIEH) mechanism.

A notable feature of Scheme 1 is that both the DPEH and IIEH mechanisms are connected together by the association/dissociation of the electroinactive counterion. Thus in addition to the ion pairs versus ions involved in the electron-hopping process, the coupling between the electroinactive ion displacement and the electron-hopping process is also different between these two mechanisms.[25] This feature makes the IIEH mechanism thermodynamically more favorable than the DPEH mechanism. However, since the actual mechanism that controls a particular electron transport process is kinetically controlled, under normal circumstances IIEH prevails over DPEH due to thermodynamic suitability. As a consequence of extensive ion pairing, the charge transport rate tends to become low, and under this condition, the IIEH mechanism is likely to be replaced by the kinetically favored DPEH mechanism. Thus both these processes operate in tandem to transport charges across the supramolecular structure.

When the IIEH mechanism is operative, the flux for the apparent motion of O^+ is written using a second-order law derived from the bimolecular characteristics of electron hopping as (cf. part 1)

$$-J_{O^+} = D_E\left\{\chi_R \frac{\partial \chi_{O^+}}{\partial x} - \chi_{O^+}\frac{\partial \chi_R}{\partial x} + \frac{ne}{k_B T}\chi_{O^+}\chi_R \frac{\partial \phi}{\partial x}\right\} \quad (1)$$

and for the movement of reduced species,

$$-J_R = D_E\left\{\chi_{O^+} \frac{\partial \chi_R}{\partial x} - \chi_R\frac{\partial \chi_{O^+}}{\partial x} - \frac{ne}{k_B T}\chi_{O^+}\chi_R \frac{\partial \phi}{\partial x}\right\} \quad (2)$$

While electron hopping leads to charge propagation, counterions move appropriately in order to maintain the system electrically neutral. The steady-state equation for the movement of free counterions described by the classical Nernst−Planck equation is[40]

$$-J_c = D_c\left\{\frac{\partial \chi_c^{\ F}}{\partial x} + \frac{z_c e}{k_B T}\chi_c^{\ F}\frac{\partial \phi}{\partial x}\right\} \quad (3)$$

The experimental conditions can be adjusted such that it is possible to study the movement of charged species under two different forces, namely, (i) potential and concentration gradient driven transport and (ii) potential gradient alone. For example, in alternating current (ac) techniques there are two frequency regimes[20] with characteristically different conductance behaviors: firstly, the lower frequency Warburg regime characterized by nonuniform potential and concentration profiles. Thus the charged species movement takes place by coupled diffusion−migration, and this regime is essentially concentration polarized. The other region is the high-frequency regime, which is the geometric, normal Kohlrausch law regime, and each charged species moves independently through the uniform concentration of electrolyte. In this, no concentration gradient exists and individual ions move independently in the dilute solution limit. In the present model, we essentially concentrate on the conductance variation in the Kohlrausch law regime (not necessarily for systems studied under ac techniques) and study the effect of ion pairing and diffusivity of electrons and counterions on conductance and transport number variations. It is also possible to construct appropriate transmission line models[20,21] so as to delineate the contribution from each dynamical process.

Using Onsager's irreversible thermodynamics formalism,[41,42] the fluxes and forces can be represented as

$$J_R = L_{RR}X_R + L_{RO^+}X_{O^+} \quad (4)$$

$$J_{O^+} = L_{O^+R}X_R + L_{O^+O^+}X_{O^+} \quad (5)$$

and the validity of the reciprocity relation implies $L_{O^+R} = L_{RO^+}$ and $L_{O^+O^+} = -L_{O^+R} = L_{RR}$; thus,

$$J_R = L_{RR}(X_{O^+} - X_R) \quad (6)$$

$$J_{O^+} = -L_{RR}(X_R - X_{O^+}) \quad (7)$$

Under the Kohlrausch law regime,[20] when concentration gradients are absent, the flux is governed only by the electrical gradient. The generalized forces and fluxes can be written in terms of the potential gradient as

$$J_R = neL_{RR}\frac{\partial \Psi}{\partial x} \tag{8}$$

$$J_{O^+} = -neL_{RR}\frac{\partial \Psi}{\partial x} \tag{9}$$

where $z_{O^+} - z_R = n$. Onsager's cross-phenomenological coefficient, L_{O^+R}, in terms of the conventional diffusion coefficient (cf. eq 19 of part 1) is

$$L_{RR} = \frac{D_{hop}}{k_B T}\chi_{O^+}\chi_R C_T \tag{10}$$

Thus the flux equations become

$$J_R = \frac{neD_{hop}}{k_B T}\chi_{O^+}\chi_R C_T \frac{\partial \Psi}{\partial x} \tag{11}$$

$$J_{O^+} = \frac{neD_{hop}}{k_B T}\chi_{O^+}\chi_R C_T \frac{\partial \Psi}{\partial x} \tag{12}$$

From the IIEH mechanism in Scheme 1, it is obvious that not all the oxidized species concentration, χ_o, are involved in the electron self-exchange with reduced species (χ_R) but only a portion of oxidized species that exist as ions (χ_{O^+}). The concentration of χ_{O^+} is governed by the ion association equilibrium constant K_{as},

$$K_{as} = \frac{\chi_O}{\chi_O + \chi_c{}^F C_T} \tag{13}$$

where $\chi_c{}^F$ is the fraction of free counterions. The conservation of oxidized species implies that

$$\chi_O{}^T = \chi_O + \chi_{O^+} \tag{14}$$

and $\chi_{O^+} = \chi_c{}^F$. The conservation of electroactive species implies that

$$\chi_R{}^T + \chi_O{}^T = 1 \tag{15}$$

where $\chi_R{}^T = \chi_R$. In the absence of supporting electrolyte, only free counterions that are not involved in ion pairing with electroactive species can move inside the polymeric matrix. Under the electrical gradient condition the flux due to free counterions is expressed using the Nernst−Planck equation as

$$J_c = -\frac{z_c e D_c}{k_B T}\chi_c{}^F C_T \frac{\partial \Psi}{\partial x} \tag{16}$$

The conductivity equation using irreversible thermodynamics concept is

$$\kappa_{ec} = \frac{-e\sum_i z_i J_i}{(d\Psi/dx)} \qquad i = O^+, R, c \tag{17}$$

Substituting appropriate J_i's, we obtain

$$\kappa_{ec} = \frac{e^2 C_T}{k_B T}(n^2\chi_{O^+}\chi_R D_{hop} + z_c{}^2\chi_c{}^F D_c) \tag{18}$$

where $\chi_x{}^F = C_x{}^F/C_T$. From eq 18, two limiting cases, viz., electron transport and ion transport controls, can be envisaged based on the system parameters, indicating that charge-transfer conductivity depends not only on the electron-transfer dynamics but also on the movement of counterions. According to Buck's terminology, this equation can also be called high-frequency specific conductivity in view of its one-to-one correspondence with eq 28 of ref 27.

The above equation is a generalized expression for conductivity in the absence of supporting electrolyte. In an electrolyte solution however, fluxes due to anions and cations of the supporting electrolyte also influence the conductivity: the greater their concentration, the greater the conductivity will be. Conductance of electrolyte solutions can also be written using the Nernst−Planck equation as

$$\kappa^\circ = \frac{e^2 C_T \chi^\circ}{k_B T}(z_y{}^2 \upsilon_y D_y{}^\circ + z_z{}^2 \upsilon_z D_z{}^\circ) \tag{19}$$

where $\chi^\circ = C^\circ/C_T$, υ_y and υ_z denote the moles of anions and cations per mole of the associated electrolyte in the electrolyte bath phase, $D_y{}^\circ$ and $D_z{}^\circ$ are their corresponding diffusion coefficients, and C° is the concentration of the binary electrolyte.

We can define appropriate transport numbers relevant in this context as

$$t_i = \frac{z_i J_i}{\sum_i z_i J_i} \qquad i = O^+, R, c \tag{20}$$

The transference number of oxidized and reduced species for electrons and counterions in the absence of supporting electrolyte represented by t_o, t_R, t_e, and t_c respectively are therefore as follows:

$$t_{O^+} = \frac{z_{O^+} n\chi_{O^+}\chi_R D_{hop}}{(n^2\chi_{O^+}\chi_R D_{hop} + z_c{}^2\chi_c{}^F D_c)} \tag{21}$$

$$t_R = \frac{-z_R n\chi_{O^+}\chi_R D_{hop}}{(n^2\chi_{O^+}\chi_R D_{hop} + z_c{}^2\chi_c{}^F D_c)} \tag{22}$$

$$t_e = t_{O^+} + t_R = \frac{n^2\chi_{O^+}\chi_R D_{hop}}{(n^2\chi_{O^+}\chi_R D_{hop} + z_c{}^2\chi_c{}^F D_c)} \tag{23}$$

$$t_c = \frac{z_c{}^2\chi_c{}^F D_c}{(n^2\chi_{O^+}\chi_R D_{hop} + z_c{}^2\chi_c{}^F D_c)} \tag{24}$$

where t_e refers to the transport number for electron hopping.

In the Absence of Supporting Electrolyte. The conductivity and the transport number plots are obtained by solving eqs 13 and 14 for χ_{O^+} and substituting these in the appropriate equations. The potential is expressed using the Nernst law and made dimensionless as $(E - E_0)ne/k_B T$. Several plots are generated by substituting diverse values for $\sigma = K_{as}C_T$ in eq 13 and $D = D_{hop}/D_c$ in eq 18. Dimensionless conductance (ξ) corresponds to $\kappa_{ec}k_B T/e^2 D_c C_T$.

We assume in this analysis that D_{hop} is independent of potential, and consequently D is constant. In addition we also

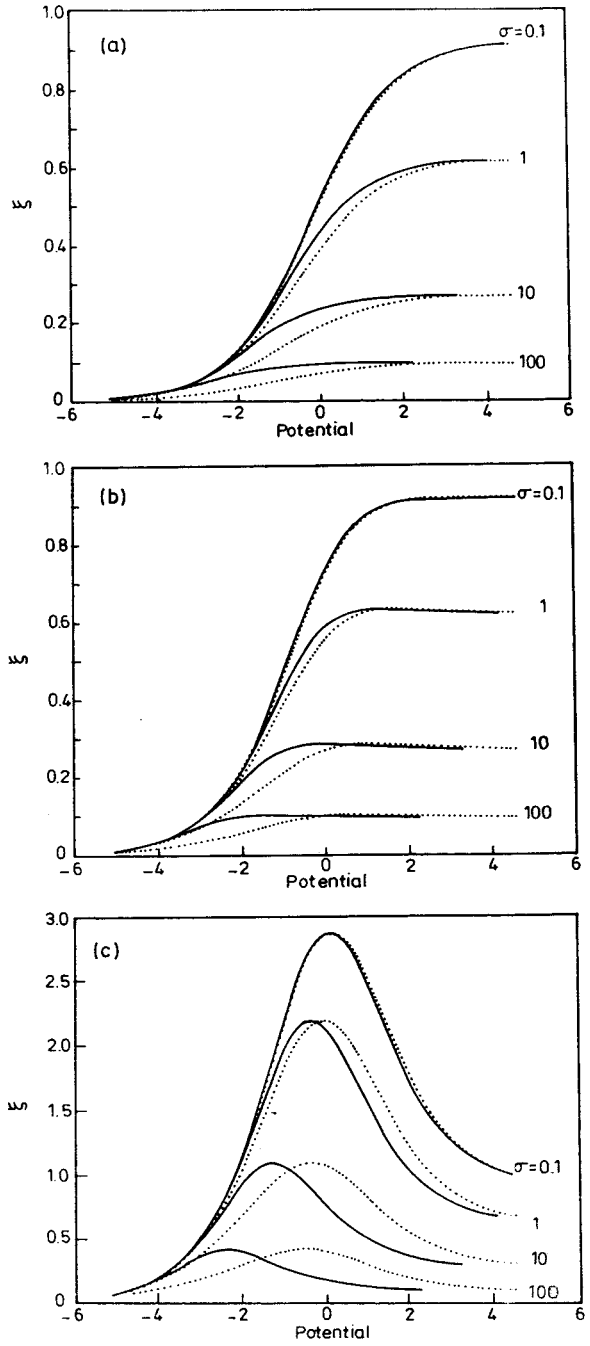

Figure 1. Variation of dimensionless conductance with potential for D values 0.1 (a), 1 (b), and 10 (c). Solid lines indicate the numerical results obtained for the indicated σ values, and dotted lines represent the conductance behavior when potential is assumed independent of ion pairing.

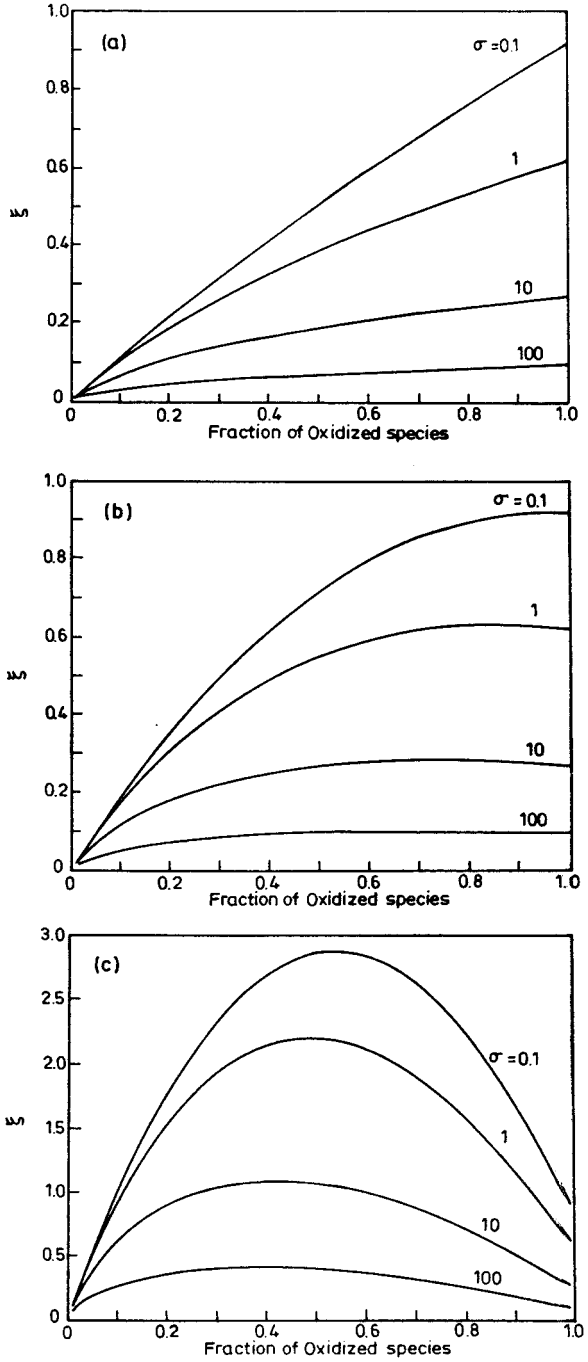

Figure 2. Dependence of dimensionless conductance on the fractional concentration of the oxidized species, ion pairing constant (σ), and ratio of diffusivity (D). The plots are obtained for D values 0.1 (a), 1 (b), and 10 (c) and for the indicated σ values.

assume that χ_T, i.e., the total concentration of the electroactive species, is above the percolation threshold. If χ_T is less than the percolation threshold, then the site−site movement or the segmental motion of the redox centers also needs to be considered to interpret the conductance behavior. Under this condition, the rate of charge transfer is controlled by site-to-site movement, and the conductance behavior will be more complicated.

Figure 1 depicts the variation of dimensionless conductance with potential for different values of D_{hop}/D_c denoted here as D for brevity. It can be seen that as D varies from 0.1 to 1, there is a gradual transition from ohmic to nonohmic behavior. Further, the absolute value of conductance ξ is also enhanced appreciably when D_{hop}/D_c is altered. Figure 2, which should be viewed in conjunction with Figure 1, depicts an analogous behavior concerning ohmic-to-nonohmic transition, when the fraction of electroactive centers is changed. The linearity between conductance and the fraction of redox centers indicating the onset of ohmic pattern is depicted even more clearly in Figure 2a for small values of D with different values of the ion-pairing equilibrium constant. Figure 2b,c indicates the effect of varying D on the transition to nonohmic. Further, Figure 2c displays a maximum in conductance when a particular concentration of redox sites is reached, and for values of σ lower than 0.1 and for $\sigma \geq 100$, the conductance reaches a plateau for any given D.

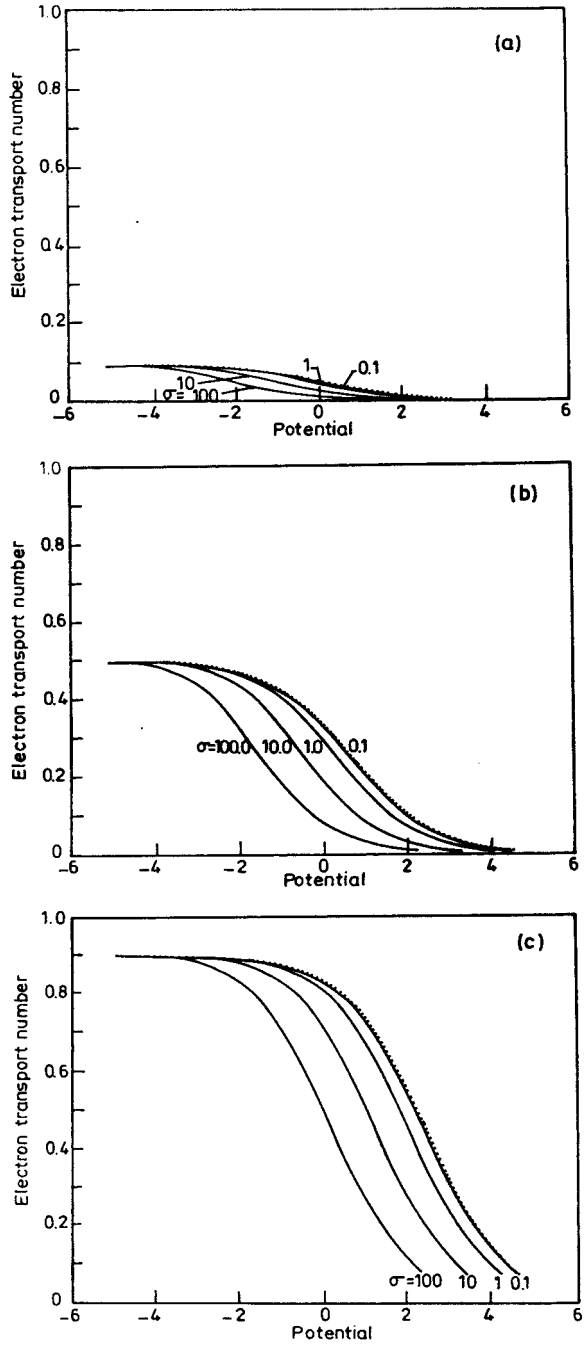

Figure 3. Variation of electron transport number with electrode potential. Dotted line defines the limiting case when potential is independent of ion pairing. The *D* values 0.1 (a), 1 (b), and 10 (c) dictate the competition between electron hopping and counterion movement.

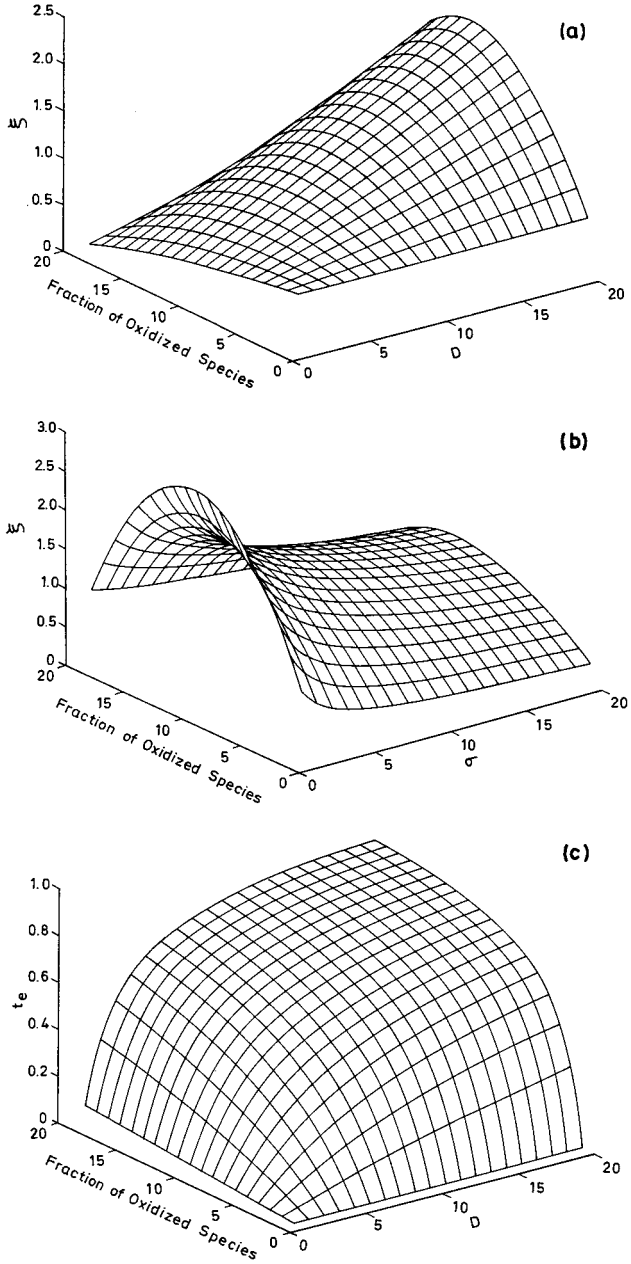

Figure 4. Dependence of dimensionless conductance (a) and electron transport number (c) on fractional concentration of the oxidized species and diffusion coefficient ratio for an ion-pairing constant value of 0.1. Mesh plot (b) depicts the variation of dimensionless conductance with fractional concentration and σ for a *D* value of 10. The range of values chosen for the mesh plot are 0.1:0.05:1, 0.1:0.5:10, and 0.1:0.25:10 for potential, *D*, and σ, respectively. The numbers indicated on the *x* and *y* axis correspond to the *i*th value in the range chosen.

Another important parametric dependence that needs to be deciphered is the influence of potential when competing transport processes, viz., electron hopping and counterion movement, occur. Figure 3 illustrates the variation of t_e with potential for different values of σ. As anticipated, a high value of electron transport number is obtained when D_{hop}/D_c is large. As the value of σ is increased, the deviation in the potential axis also increases, suggesting that the effect of ion pairing is to shift the potential to more negative values. This can also be seen from Figure 3a. The analysis will become more illuminating if we resort to a three-dimensional pictorial representation of these plots. The cumulative effect of ion pairing constants, diffusivity ratio, and fractional concentration of oxidized species on the observed dimensionless conductance is depicted in Figure 4a,b.

Whenever $\sigma < < 0.1$, the conductance and transport number curves remain unchanged owing to the complete dissociation of the oxidized species under this condition; that is, χ_O^T becomes approximately equal to χ_{O^+}, and hence any further decrease in this value has no effect on the conductance or transport number. As in the earlier plot of dimensionless conductance with regard to diffusivity ratio and fractional concentration, a 3D mesh plot depicting the transport number variation with respect to the two system variables is shown in Figure 4c. For subsequent increases in *D*, the electron transport number slowly increases

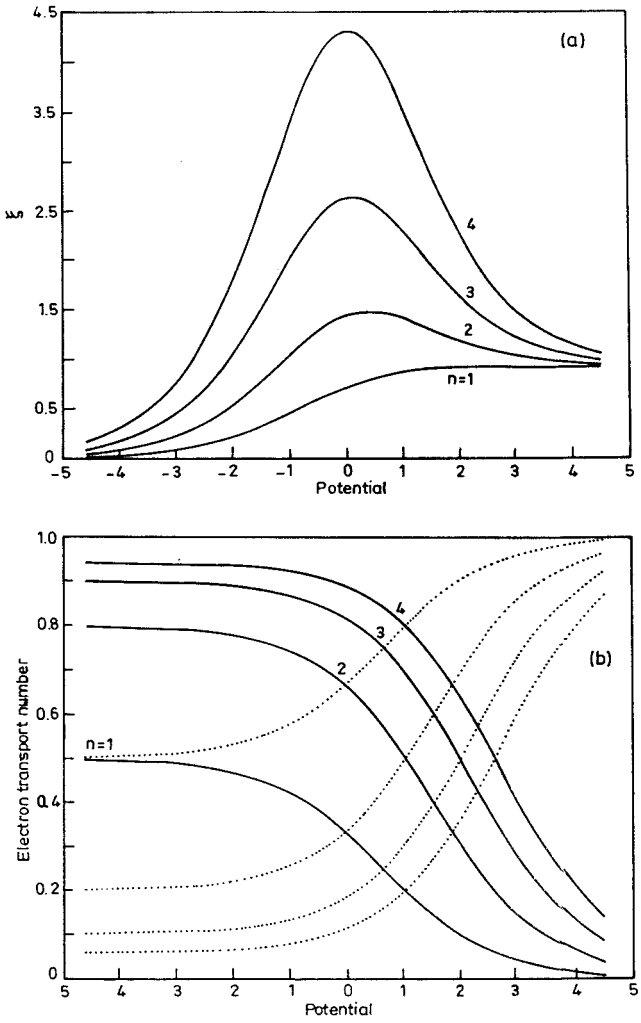

Figure 5. Variation of dimensionless conductance (a) and electron transport number (b) with electrode potential and number of electrons transferred for $\sigma = 0.1$ and $D = 1$. In b, dotted lines correspond to the counterion transport number.

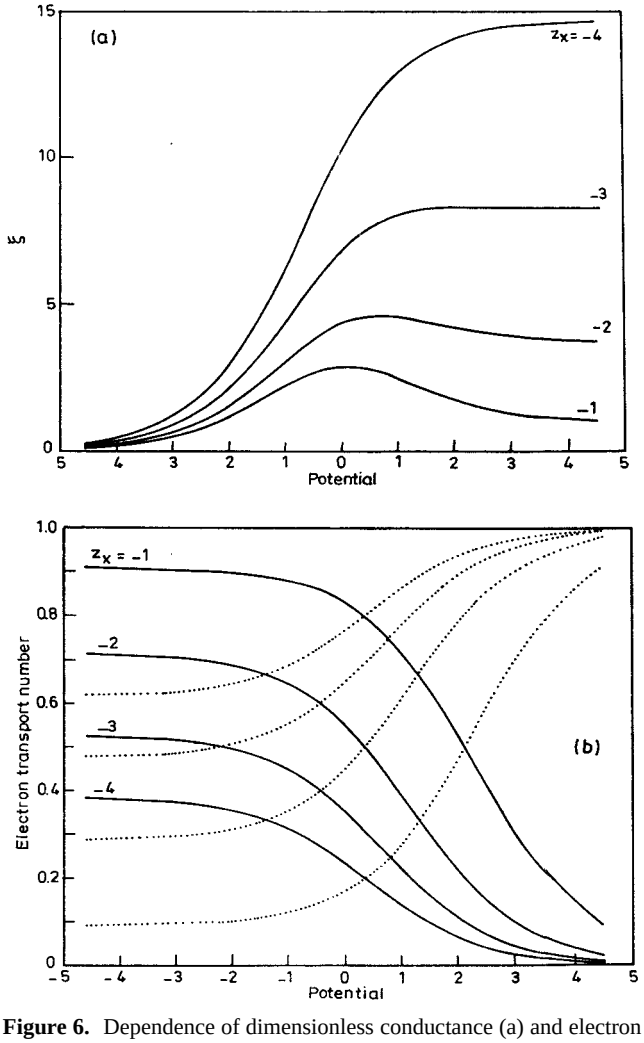

Figure 6. Dependence of dimensionless conductance (a) and electron transport number (b) on the electrode potential and charge on the counterion for $\sigma = 0.1$ and $D = 10$. In b, dotted lines correspond to the counterion transport number.

and attains unity and becomes independent of potential at higher values of D, indicating that the system becomes counterion transfer controlled.

It is customary[43] to employ polyvalent redox couples in studies involving chemically modified electrodes, and therefore one may enquire how the number of electrons transferred influences conductance behavior. It is seen from Figure 5a that when $n = 1$, the absolute value of ξ is smaller and reaches a plateau for large positive values of potential, whereas for $n \neq 1$, a maximum in conductance is observed. The physical origin of such a behavior may be ascribed to the numerically higher charge carried by the species as well as the change in the rate-controlling process. The plot depicted in Figure 5a for the case of $n = 1$ is reminiscent of Figure 1b, where also ohmic behavior is noticed if $\sigma = 0.1$ and the ratio of diffusion coefficients equals unity. A pronounced departure from ohmic law is noted as n increases. Analogously, Figure 5b indicates the variation of electron transport number for different n. Further, the counterion transport number and electron transport number behave in an opposite manner (as a function of potential), and the sum of the two has to be unity.

Thus far, we have illustrated the influence of D, n, and σ on conductance behavior and transport numbers (t_e and t_c). It is imperative at this stage to analyze the dependence of ξ, t_e, t_c, etc., on the charge of the counterions employed. Figure 6a illustrates the patterns of conductance decrease when z_c is varied. This is, once again, in conformity with Figure 5a, where an increase in n leads to enhanced conductance values. The insights obtained from Figure 6a need to be compared with those resulting from Figure 1c. In the case of Figure 1c, when $D = 10$, $\sigma = 0.1$, $n = 1$, and $z_c = -1$, nonohmic behavior is noticed, whereas in Figure 6a, as z_c is increased, linear conductance variation is observed for the same value of D, and σ, thereby showing the marked influence of counterion charges on the mechanism of charge transport. Figure 6b demonstrates that the electron transport number is large when the counterion charge is low.

The schematic plots given in Figures 1−6 indicate that one may obtain a maximum value of dimensionless conductance by varying appropriately the parameters D_{hop}, D_c, n, z_c, and σ. It is instructive to obtain an insight into the maximum value of ξ as a function of the above system parameters. For this purpose, a plot of ξ_{max} versus log σ for different D values is shown in Figure 7 and is in agreement with Figure 1, which predicts a pronounced increase in ξ_{max} for large D. Similar plots depicting identical features of maximum conductance with log σ are reported by Saveant[24] by numerically solving the diffusion−migration equation but for the ion transport controlled process. The present study illustrates that this feature remains the same for the activation-controlled process as well (Figure 7). The concentration of the oxidized species where ξ_{max} is

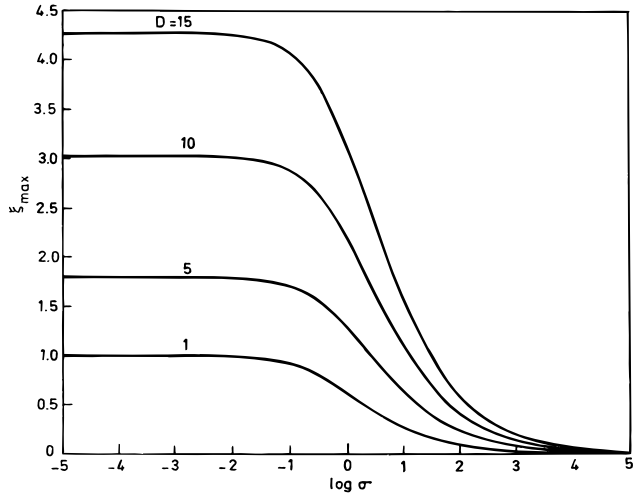

Figure 7. Conductance maximum as a function of the extent of ion pairing for the indicated D values.

TABLE 1: Variation of Mixed Valent Region Concentration ($\chi_{O,Max}^{T}$) with D in the Absence of Supporting Electrolyte

D	$\chi_{O,M}^{T}$ [a]
0.1	1.00
1	1.00−0.67
5	0.60−0.40
10	0.55−0.37
15	0.53−0.36
100	0.50−0.34
1000	0.50−0.33

[a] The range of $\chi_{O,Max}^{T}$ is given for σ ranging between 10^{-5} and 10^{5}.

observed in the nonohmic region is termed by Murray as the mixed valent concentration ($\chi_{O,Max}^{T}$).[44] This mixed valent region is defined to be the region at which the oxidized and reduced species concentrations are identical. However $\chi_{O,Max}^{T}$ is found to be a function of both σ and D in the present study. For ohmic behavior, the maximum conductivity is observed when $\chi_{O,Max}^{T} = 1$ as expected, whereas in the nonohmic region the mixed valent region varies with D value as shown in Table 1. The value of $\chi_{O,Max}^{T}$ also gives a clue about the nature of the conductance process.

Influence of Supporting Electrolyte. The dimensionless plots of conductance (ξ) against potential in the presence of supporting electrolyte are shown in Figures 8 and 9. These are obtained by incorporating the conductance contribution from the binary electrolyte (eq 19) in eq 18 and assuming the ionic diffusivities of a 1:1 electrolyte as identical. The conductance plots shown here are apparently similar to those observed in the absence of supporting electrolyte. The supporting electrolyte has no effect on the conductance plot until a threshold concentration is reached, beyond which the conductance increases *albeit* slowly. Here too, the effect of the ion-pairing association constant decreases the conductance value and shifts the conductance plot in the negative direction on the potential axis. Figure 8a depicts the expected pattern of ξ in the presence of supporting electrolyte for various D estimates. A small increase in the maximum value of conductance is noticed in this case in contrast to Figure 1a. The linear and the parabolic dependences of conductance on the oxidized species concentration are shown in Figure 8b.

Figure 9 indicates the effect of varying D on conductance behavior when χ^0 is held constant. It is to be emphasized that when D is large, conductance shows a maximum irrespective of σ chosen *and* its magnitude is large. The latter behavior is

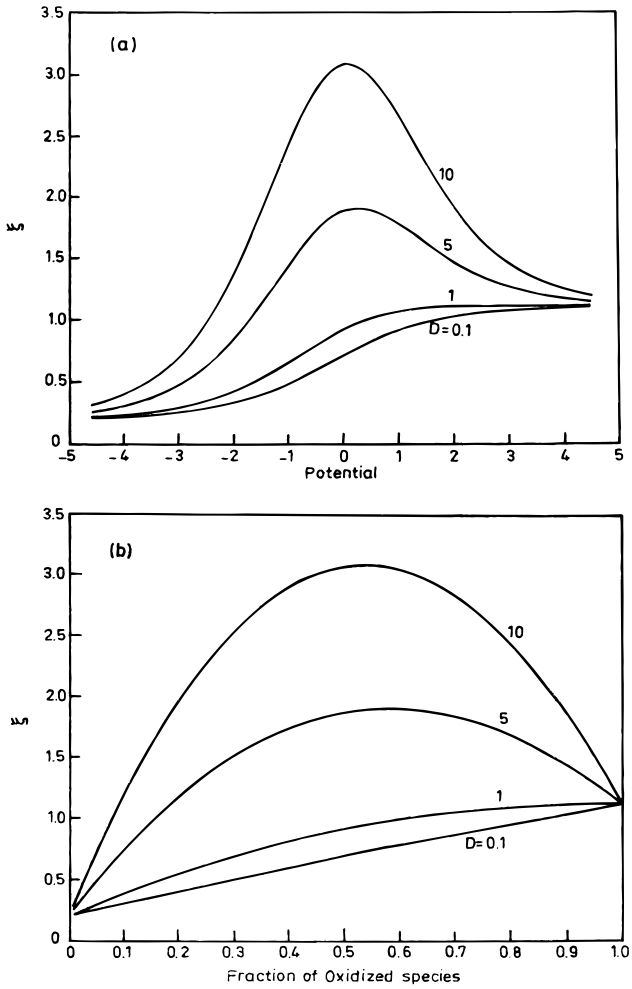

Figure 8. Variation of dimensionless conductance with electrode potential (a) and fractional concentration of oxidized species (b). The values indicated correspond to D and for $\sigma = 0.1$ and $\chi^0 = 0.1$.

not entirely fortuitous since the Nernst−Einstein mobility relation also predicts this trend. Figure 10 indicates the dependence of t_e and t_c upon potential for D ranging from 0.1 to 100, for two representative values of ion-pairing association constants. As mentioned earlier, the behavior of t_e and t_c are diametrically opposite each other, at all potentials. An important difference concerning t_e and t_c variations with potential between the presence of supporting electrolyte and its absence needs to be emphasized. In Figure 3 of Buck,[29] t_e versus mole fraction of reduced species exhibits a maximum in the absence of supporting electrolyte *as well as* ion pairing, whereas Figure 10a yields a similar behavior when the ion-pairing association constant is 0.1 and in the presence of supporting electrolyte.

Further, electron transport number−potential plots of Figure 10a for various values of D when $\sigma = 0.1$ and $\chi^0 = 0.1$ show a marked difference from Figure 3 obtained in the absence of supporting electrolyte discussed earlier. Here, the electron-transfer control is observed for $D < 0.1$ in which the electron transport number is approximately potential independent. Similarly for $D > 100$, potential-independent behavior is again observed and the system is under ion-transfer control. For any intermediate range, such as $0.1 < D < 100$, the transference number curves show regions of mixed control. These plots are not always symmetrical but depend on the σ value for onset of symmetry. When the σ value is ≤ 0.1, the curves are symmetrical and any subsequent increase in this shifts the maximum in the transference number toward higher negative

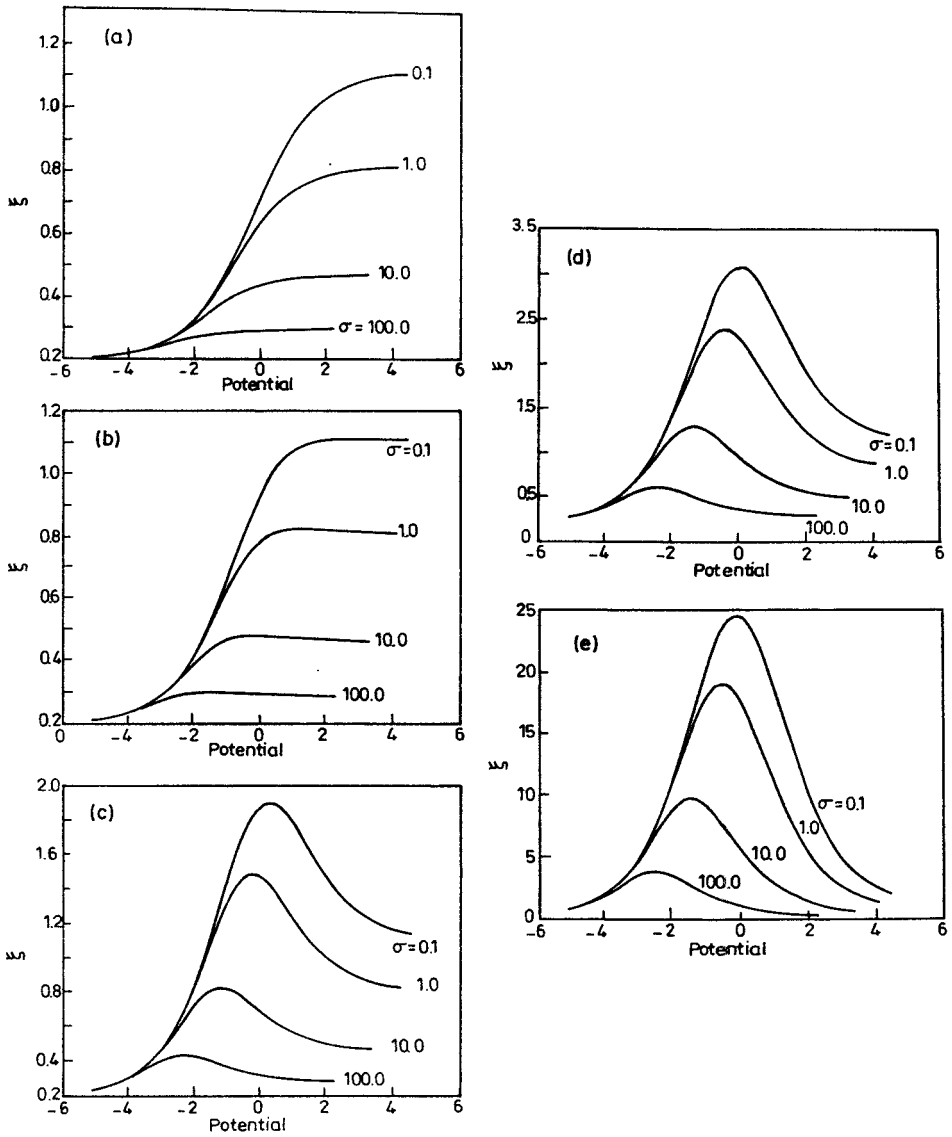

Figure 9. Variation of dimensionless conductance with potential and ion-pairing constant for D values of 0.1 (a), 1 (b), 5 (c), 10 (d), and 100 (e) ($\chi^0 = 0.1$).

potentials, and this process destroys the symmetry (Figure 10b). It can be noted that, when σ is very large, the availability of non-ion-paired redox centers decreases and hence a decrease in t_e along with a slight shift on the potential axis occurs. In addition, as the σ value increases, the system slowly moves away from the counterion transport control and mixed control and reaches electron transfer control. It is interesting to compare the shape of this plot and also the value of the transference number maximum (for increasing σ values) with the analogous ones in the absence of supporting electrolyte. Even though conductance decreases, the mechanism of the process in the absence of supporting electrolyte remains the same since the electron transport number is independent of the variables χ_{O^+} and χ_c^F. However, in the presence of supporting electrolyte, t_e depends on these variables and affects the rate-controlling process.

The higher and lower values of $\chi_{O,Max}{}^T$ shown in Table 2 are obtained when the supporting electrolyte concentration is high and low, respectively. The upper limit in the mixed valent concentration is a function of both σ and D. However, the lower limit is fixed solely by the σ value. The conductance moves toward nonohmic redox behavior when D is increased, and in that process the range of mixed valent concentrations also decreases. When the ion pairing between the attached electroactive ions and the mobile electroinactive counterions is weak, the maximum conductance is observed when the oxidized species concentration is around 0.5, as observed in the case of systems where ion-pairing effects are absent. But the lower limit reduction in $\chi_{O,Max}{}^T$ at higher values of D for the strongly ion-paired system is unexpected. Further, the range of mixed valent concentrations indicates that the concentration of supporting electrolyte also determines the nature of the conductance process. For example, when $\sigma = D = 0.1$, the conductivity observed is electronic for lower values of χ^0 and nonohmic redox at higher values. The effect of increasing the number of electrons transferred and charge of the counterions has exactly the same effect as observed in the case when supporting electrolyte is absent (cf. Figures 5, 6).

The effect of the added supporting electrolyte on charge transport dynamics can be understood by comparing Figures 10a and 11a. As the supporting electrolyte concentration is increased, two distinct features are observed in these plots. Firstly, the curve becomes more symmetrical at higher concentrations of supporting electrolyte, indicating that the mixed valent region shifts between the values indicated in Table 2. The shift in the oxidized species concentration where the maximum

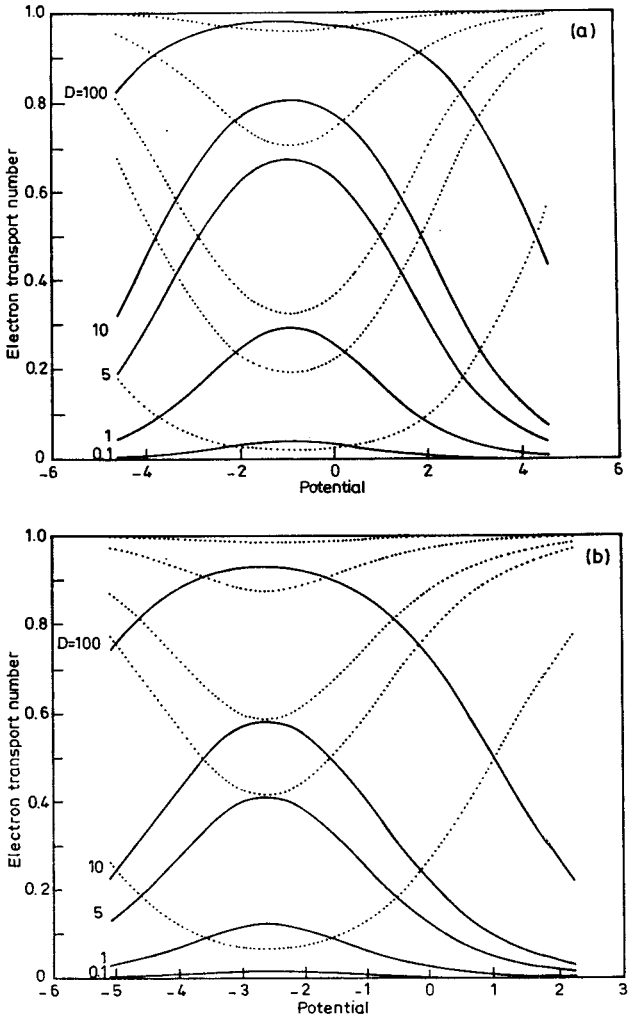

Figure 10. Electron transport number−potential curves for σ values of 0.1 (a) and 100 (b), and indicated D values ($\chi^0 = 0.1$). Dotted lines represent counterion transport number curves for the corresponding D values.

TABLE 2: Variation of Mixed Valent Region Concentration ($\chi_{O,Max}{}^T$) with D and σ Values in the Presence of Supporting Electrolyte

σ	D	$\chi^T_{O,Max}{}^a$
0.1	0.1	1.00−0.49
0.1	1	0.96−0.49
0.1	5	0.58−0.49
0.1	10	0.54−0.49
1	1	0.85−0.44
10	1	0.74−0.38
100	1	0.69−0.35

[a] The range of $\chi_{O,Max}{}^T$ is given for the supporting electrolyte concentration, χ^0, between 10^3 and 10^{-3}.

electron hopping (or equivalently minimum transport of counterions) occurs essentially accounts for the symmetry of the curve. Secondly, the increase in supporting electrolyte concentration enhances the conductance and decreases the electron transport number as expected. Thus, the addition of supporting electrolyte slowly changes the rate control from counterion movement to electron-hopping process. An exactly opposite effect has been observed when the value of D is increased as shown in Figure 11b,c.

The effect of added supporting electrolyte on the maximum conductance (ξ_{max}) in the case of both ohmic and redox regions is studied in Figure 12. A common feature of these plots is

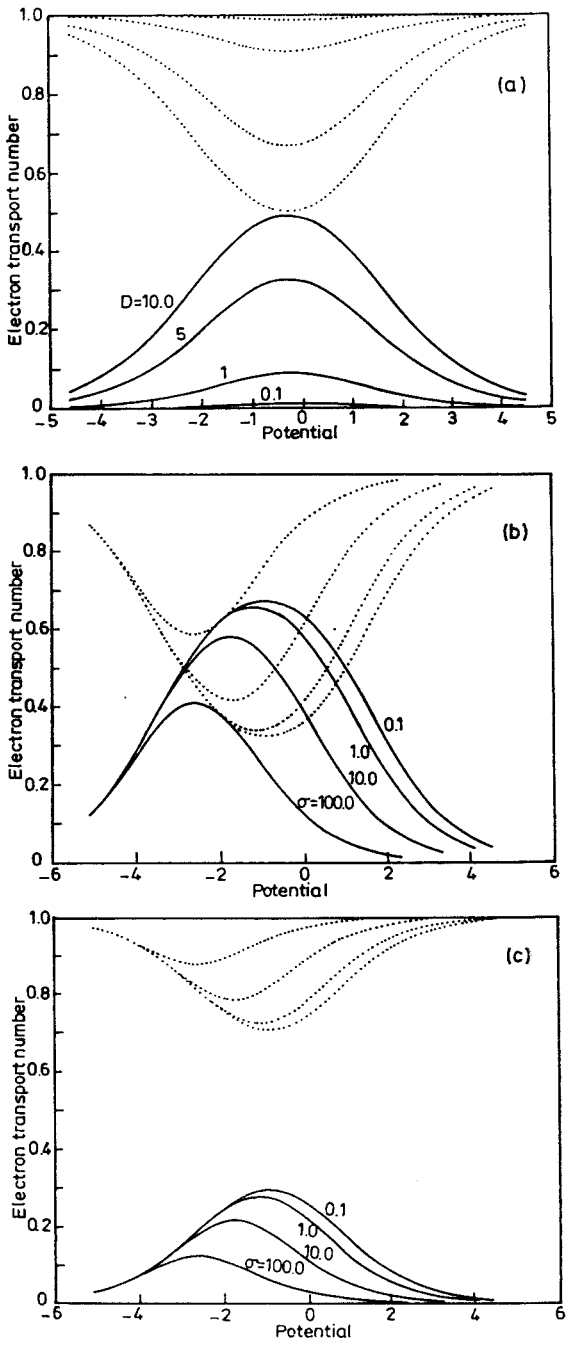

Figure 11. Electron transport number as a function of potential, when $\chi^0 = 0.1$; (a) for various values of D ($\sigma = 0.1$), (b) $D = 5$, and (c) $D = 1$ for indicated values of σ.

that the conductance maximum remains independent of the supporting electrolyte concentration until a particular threshold value is reached and beyond which conductance increases exponentially. This threshold concentration is a function of the ratio of diffusion coefficients only, and the ion-pairing equilibrium constant essentially accounts for the steeper variation in ξ_{max}.

Comparison with Existing Approaches

It is interesting to compare our Figure 10a with a similar plot reported by Mathias and Haas (Figure 4 of ref 32) for various values of D with $\chi^0 = 0.1$. The differences between these two plots are due to the ion-pairing effect. For $\sigma << 0.1$ the oxidized species present is not involved in ion pairing,

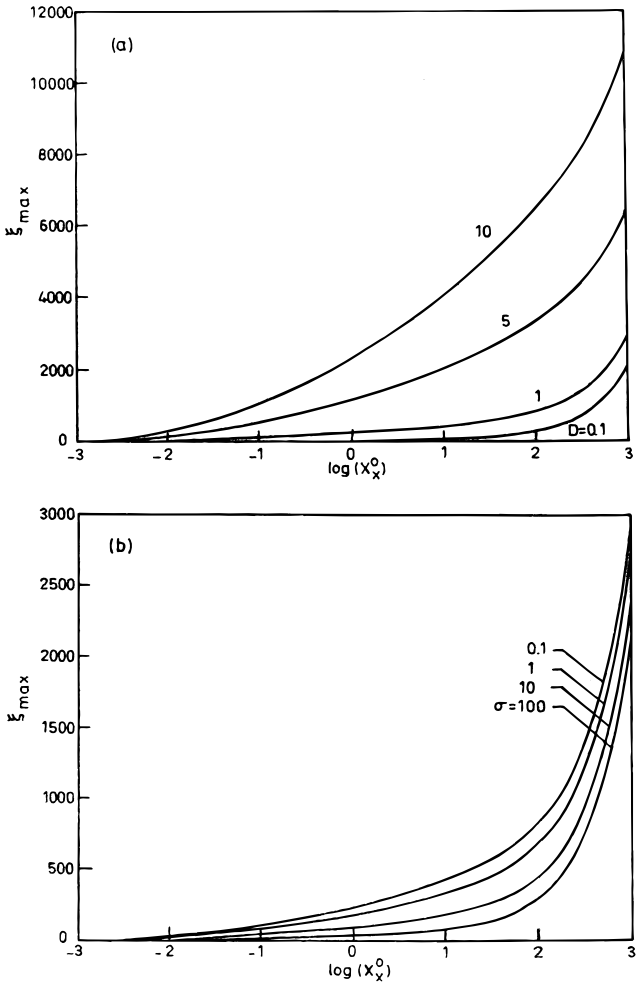

Figure 12. Maximum dimensionless conductance as a function of supporting electrolyte concentration for various values of D (a) and σ (b) shown in the figure.

and hence $\chi_O{}^T$ can be approximated to χ_{O^+} and it is expected that ion pairing will have no effect on the transport number. However when σ decreases, $\chi_c{}^F$ will also increase with χ_{O^+} (cf. eq 13), and this also contributes to the current and increases the transport number t_c (and decreases t_e). When ion pairing is assumed to be absent or when the contribution of $\chi_c{}^F$ to the charge transport is neglected, Figure 10a here becomes identical to Figure 4 of Mathias and Hass.[32]

In an earlier study, Wilbourn and Murray[45] showed that dc current−voltage characteristics conventionally associated with electronic and redox conductivity are not material-dependent phenomena but are dictated by the choice of the environment in which the conductivity measurements are made. The chosen environment modifies the system parameters, namely, the ion-pairing association constant and the diffusion coefficient ratio between electrons and counterions. This leads to different conduction mechanisms. For example, poly(benzimidazobenzophenanthroline) (BBL) film on an electrode *under electrolyte solution wetted conditions* exhibits a large thermal activation barrier, and current−voltage behavior is characteristic of redox conductors; in other words, the conductance observed is nonohmic. From low-temperature studies,[45] it is shown that counterion diffusivity is quenched more than electron diffusivity, under the experimental conditions, while the movement of the counterion, which is slow, becomes rate determining (Figure 11c). Thus the conductance observed is nonohmic as in Figure 9e).

As opposed to this, the conductance−voltage curves for copped BBL films *dried out in Ar atmosphere* gradually become linear (ohmic) conductors. The conductivity observed at this stage is smaller than the redox conductance observed under solution wetted conditions, the essential reason being that the electron diffusivity decrease is greater than the counterion movement. Thus the conductance observed is electronic, as shown in Figure 1a; the electron transport becomes rate determining and the charge transport is dominated by counterion movement, and hence ohmic behavior is noted. There is a dichotomy between the mechanism of the charge transport and the magnitude of the observed current. While the mechanism is dictated by the slower of the two processes, the magnitude of the current is not influenced by the same! The temperature variation studies also indicate an increased conductivity at higher temperatures in the presence of supporting electrolyte *both in solvent and in dry Ar conditions* due to the decrease in ion-pairing equilibrium constant. However, when the supporting electrolyte is completely removed and when conduction was studied under Ar atmosphere, an increase in conductance was observed due to long-distance electron hopping because the delocalized π bonds assist in electronic conduction.[46] Hence conductance is invariant with the counterion concentration and is also independent of temperature.

Another example where a similar behavior (without long-distance electron hopping) is observed is in the case of $[Os(vbpy)_3]^{2+}/[Zn(vbpy)_3]^{2+}$ copolymer,[47] where Zn sites are electron transfer silent and act as diluent. Here too the conductivity observed by varying Os sites concentration is found to vary with the environment. The conductivity studied using the sandwich electrode construction decreases in the progression of bath media electrolyte in the order electrolyte/CH_2Cl_2 solvent > CH_2Cl_2 vapor > dry N_2, which can easily be explained by the model proposed here.

Summary

Within the irreversible thermodynamics framework, conductance and transport numbers are studied to comprehend the behavior and control of the charge propagation in polymer-modified electrodes. The effect of mobile electroinactive counterions on the conductance and charge propagation in the polymeric region under steady-state experimental conditions is also rationalized. The control of the mobile electroinactive ions on the charge transport rate arises from the strength of the ion pairs it may create with the electroactive ion: the stronger the ion pairs, the slower the charge transport. In contrast to the argument that steady-state currents do not depend upon the diffusivity of the electroinactive counterions, the analysis carried out here shows that conductance resulting from the coupling of electron hopping between localized sites with electroinactive counterion depends on both the redox active and electroinactive counterion diffusivities: the smaller the diffusivity of the counterion, the larger the current and greater the nonohmic conductance behavior. Thus the electron hopping and electroinactive counterion displacement are coupled such that the slower of the two dominates in determining the overall rate of the process, as one anticipates intuitively.

The effect of ion pairing is felt on charge transport only when the electroinactive counterion is significantly ion paired with the electroactive ions. However, when the association is weak, the conductance and transport number behavior resembles that of the non-ion-paired system for a given ratio of diffusivities. This is evident from the "mixed valent region" concentration being observed at around 0.5 for redox behavior of conductance.

To reiterate, the following parameters influence the conductance mechanism: (i) the diffusivity of the redox transfer active centers and electroinactive counterions, (ii) number of electrons transferred between the electroactive centers, (iii) charge of the counterions, and (iv) concentration of the supporting electrolyte when steady-state potential step experiments are carried out.

Acknowledgment. We thank Prof. R. P. Buck for sending preprints of his papers and the Department of Science and Technology (DST), Government of India for financial support.

References and Notes

(1) Diaz, A. F.; Bargon, J. In *Handbook of Conducting Polymers*; Skotheim, T. J., Ed.; Marcel Dekker: New York, 1986.
(2) Inzelt, G. *In Electroanalytical Chemistry*; Bard, A. J., Ed.; Marcel Dekker: New York, 1994; Vol. 18.
(3) Murray, R. W. In *Molecular Design of Electrode Surfaces;* Murray, R. W., Ed.; John-Wiley & Sons: New York, 1992.
(4) Abruña, H. D. In *Electroresponsive Molecular and Polymeric Systems;* Skotheim, T. J., Ed.; Marcel Dekker: New York, 1988.
(5) Murray, R. W. *Annu. Rev. Mater. Sci.* **1984**, *14*, 145.
(6) Chidsey, C. E. D.; Murray, R. W. *Science* **1986**, *231*, 25.
(7) Dalton, E. F.; Surridge, N. A.; Jernigan, J. C.; Wilbourn, K. O.; Facci, J. S.; Murray, R. W. *Chem. Phys.* **1990**, *141*, 143.
(8) Skotheim, T. A., Ed. *Handbook of Conducting Polymers;* Marcel Dekker: New York, 1986; Vol. 1, p 2.
(9) Frommer, J. E.; Chances, R. R. In *Encyclopedia of Polymer Science and Engineering*, 2nd ea.; Wiley: New York, 1986; Vol. 5, pp 462-507.
(10) Marks, T. J. *Science* **1985**, *227*, 881.
(11) Young, C. L.; Whitney, D.; Vistnes, A. I.; Dalton, L. *Annu. Rev. Phys. Chem.* **1986**, *37*, 459.
(12) Pickup, P. G.; Murray, R. W. *J. Am. Chem. Soc.* **1983**, *105*, 4510.
(13) Pickup, P. G.; Kutner, W.; Leidner, C. R.; Murray, R. W. *J. Am. Chem. Soc.* **1984**, *106*, 1991.
(14) Schlenoff, J. B.; Chien, J. C. W. *J. Am. Chem. Soc.* **1987**, *109*, 6274.
(15) Chiang, C. K.; Druy, M. A.; Gau, S. C.; Heeger, A. J.; Louis, E. J.; MacDiarmid, A. G.; Park, Y. W.; Shirakawa, H. *J. Am. Chem. Soc.* **1978**, *100*, 1013.
(16) Salmon, M.; Diaz, A. F.; Logan, A. J.; Krounbi, M.; Bargon, *J. Mol. Cryst. Liq. Cryst.* **1982**, *83*, 265.
(17) Sichel, E. K.; Knowles, M.; Rubner, M. Georger, J., Jr. *Phys. Rev. B* **1982**, *25*, 5574.
(18) Hanson, L. K.; Carneiro, K. *Mol. Cryst. Liq. Cryst.* **1985**, *119*, 471.
(19) Druy, M. A.; Rubner, M. F.; Sichel, E. K.; Tripathy, S. K.; Emma, T.; Cukor, P. *Mol. Cryst. Liq. Cryst.* **1984**, *105*, 109.
(20) Buck, R. P.; Mundt, C. *J. Chem. Soc., Faraday Trans.* **1996**, *92*, 3947.
(21) Buck, R. P.; Mundt, C. *J. Chem. Soc., Faraday Trans.* **1996**, *92*, 4987.
(22) Savéant, J.-M. *J. Electroanal. Chem.* **1988**, *262*, 1.
(23) Savéant, J.-M. *J. Phys. Chem.* **1988**, *92*, 1011.
(24) Savéant, J.-M. *J. Phys. Chem.* **1988**, *92*, 4526.
(25) Anson, F. C.; Blauch, D. N.; Savéant, J.-M.; Shu, C. F. *J. Am. Chem. Soc.* **1991**, *113*, 1922.
(26) Savéant, J.-M. *J. Electroanal. Chem.* **1988**, *242*, 1.
(27) Buck, R. P. *J. Phys. Chem.* **1988**, *92*, 4196.
(28) Buck, R. P. *J. Phys. Chem.* **1988**, *92*, 6445.
(29) Buck, R. P. *J. Electroanal. Chem.* **1989**, *258*, 1.
(30) Buck, R. P.; Mădăraş, M. B.; Mäckel, R. *J. Electroanal. Chem.* **1993**, *362*, 33.
(31) Nahir, M.; Buck, R. P. *J. Phys. Chem.* **1993**, *97*, 12362.
(32) Mathias, M. F.; Haas, O. *J. Phys. Chem.* **1992**, *96*, 3174.
(33) Mathias, M. F.; Haas, O. *J. Phys. Chem.* **1993**, *97*, 9217.
(34) Forster, J. R.; Kelly, A. J.; Vos, J. G.; Lyons, M. E. G. *J. Electroanal. Chem.* **1989**, *270*, 365.
(35) Lyons, M. E. G.; Fay, H. G.; McCabe, T.; Corish, J.; Vos, J. G.; Kelly, A. J. *J. Chem. Soc., Faraday Trans.* **1990**, *86*, 2905.
(36) Forster, R. J.; Vos, J. G. *Electrochim. Acta* **1992**, *37*, 159.
(37) Kaufman, F. B.; Schroeder, A. H.; Engler, E. M.; Kramer, S. R.; Chambers, J. Q. *J. Am. Chem. Soc.* **1980**, *102*, 483.
(38) Eisenberg, A. *Macromolecules* **1970**, *3*, 147.
(39) Eisenberg, A.; King M. In *Ion-Containing Polymers;* Academic: New York, 1977.
(40) Buck, R. P. *J. Membr. Sci.* **1984**, *17*, 1.
(41) De Groot, S. R.; Mazur, S. P. *Non-equilibrium Thermodynamics;* North-Holland: Amsterdam, 1962.
(42) Haase, R. In *Thermodynamics of Irreversible Processes*, Addison-Wesley, Reading, MA 1969.
(43) Baldy, C. J.; Elliott, C. M.; Feldberg, S. W. *J. Electroanal. Chem.* **1990**, *283*, 53.
(44) The mixed valent region is essentially defined only for nonohmic conductance. In the present study we have assumed the definition to be valid for ohmic conductance as well, even though the concentration of the redox species under this condition is not strictly mixed valent.
(45) Wilbourn, K.; Murray, R. W. *J. Phys. Chem.* **1988**, *92*, 3642.
(46) Heeger, A. J.; Kivelson, S.; Schrieffer, J. R.; Su, W.-P. *Rev. Mod. Phys.* **1988**, *60*, 781.
(47) Sosnoff, C. S.; Sullivan, M.; Murray, R. W. *J. Phys. Chem.* **1994**, *98*, 13643.